Nano Research
2020, 13(4): 1013–1019
ISSN 1998-0124 CN 11-5974/O4
https://doi.org/10.1007/s12274-020-2736-6

Research Article

Super-assembled core–shell mesoporous silica-metal-phenolic network nanoparticles for combinatorial photothermal therapy and chemotherapy

Bo Yang[1], Shan Zhou[1], Jie Zeng[1], Liping Zhang[1], Runhao Zhang[1], Kang Liang[2], Lei Xie[1], Bing Shao[3], Shaoli Song[4], Gang Huang[5,6], Dongyuan Zhao[1], Pu Chen[7], and Biao Kong[1] (✉)

[1] *Department of Chemistry, Shanghai Key Lab of Molecular Catalysis and Innovative Materials, iChEM, Fudan University, Shanghai 200032, China*
[2] *School of Chemical Engineering and Graduate School of Biomedical Engineering, The University of New South Wales, NSW 2052, Australia*
[3] *Beijing Key Laboratory of Diagnostic and Traceability Technologies for Food Poisoning, Beijing Center for Disease Prevention and Control, Beijing 100013, China*
[4] *Department of Nuclear Medicine, Shanghai Cancer Center, Fudan University, Shanghai 200032, China*
[5] *Shanghai Key Laboratory of Molecular Imaging, Shanghai University of Medicine and Health Sciences, Shanghai 201318, China*
[6] *Institute of Clinical Nuclear Medicine, Renji Hospital, Shanghai Jiao Tong University School of Medicine, Shanghai 200127, China*
[7] *Department of Chemical Engineering, University of Waterloo, Waterloo, Ontario, N2L 3G1, Canada*

Received: 10 November 2019 / **Revised:** 23 February 2020 / **Accepted:** 25 February 2020

ABSTRACT

Multimodal combinatorial therapy merges different modes of therapies in one platform, which can overcome several clinical challenges such as premature drug loss during blood circulation and significantly improve treatment efficiency. Here we report a combinatorial therapy nanoplatform that enables dual photothermal therapy and pH-stimulus-responsive chemotherapy. By super-assembly of mesoporous silica nanoparticles (MSN) with metal-phenolic networks (MPN), anti-cancer drugs can be loaded in the MSN matrix, while the outer MPN coating allows dual photothermal and pH-responsive properties. Upon near-infrared light irradiation, the MSN@MPN nanoplatform exhibits excellent photothermal effect, and demonstrates outstanding pH-triggered drug release property. *In vitro* cell experiments suggest the MSN@MPN system exhibits superior biocompatibility and can effectively kill tumor cells after loading anti-cancer drugs. Consequently, the MSN@MPN system shows promising prospects in clinical application for tumor therapy.

KEYWORDS

pH-responsive, photothermal therapy, metal-polyphenol complex, synergistic therapy

1 Introduction

Despite the significant progress made in the diagnosis and treatment of cancer, it still remains as one of the serious diseases that threaten humanity with an increasing morbidity and mortality [1–3]. Traditional single-mode therapy is considered inefficient for completely curing or inhibiting the solid tumors [4, 5]. It remains an unmet challenge to develop therapies to cure cancers more effectively. Thus, combinatorial nanotherapy that integrates multiple therapeutic functions into one nanoplatform has been proposed as a promising multi-modal cancer therapy. Combinatorial therapy highlights not only high specificity and low risk of recurrence but also shows the advantage by integrating multiple therapeutic functions into one nanoplatform [6–9].

Due to the heterogeneous microenvironments found in tissues, such as different pH or GSH levels, stimuli-responsive chemotherapy has recently attracted much attention [10–12]. A range of triggers including pH [10, 11, 13], enzyme [14, 15], temperature [16, 17], redox [18], light [19] and magnetic [20] have been exploited in stimuli-responsive chemotherapy nanosystems. Because of the acidic microenvironment (pH 5.6–6.5) that has been found in tumor tissues [21, 22], pH-responsive chemotherapy is generally regarded as the most reliable and promising technique for stimuli-responsive tumor therapy.

So far, chemotherapy combining with some emerging therapy techniques such as photothermal therapy [23–27], magnetocaloric therapy [28–30] and immunotherapy [31–34] have proven to be advantageous. Among them, photothermal therapy (PTT) shows great potential in clinical settings due to its properties of high selectivity, noninvasiveness, minimal damage to adjacent normal tissues and fast recovery [35]. The mechanism of PTT mainly includes two aspects: (i) selective aggregation of photothermal agents at the tumor tissue and (ii) the photothermal agents absorb and covert near infrared (NIR) incident light into localized thermal energy to damage or kill tumor cells [2, 36]. However, the poor bio-safety, complex synthetic process and toxic additives of PTT agents limit their advanced applications. It is imperative to develop a new type of PTT reagent to conquer these challenges.

Address correspondence to bkong@fudan.edu.cn

In this work, a dual pH and photothermal-responsive nano-carrier was fabricated via a simple and rapid super-assembly approach. As shown in Fig. 1, a core–shell nano-composite composed of a mesoporous silica nanoparticle (MSN) as the porous matrix for hosting small molecular drug and a pH and photothermal-responsive metal-tannic acid complex shell is developed (MSN@MPN). Tannic acid (TA) is a dendritic polyphenol extracted from green tea, which can be rapidly deposited and complexed with metal ions (Fe^{III}/Al^{III}) to form a coordination film on the surface of MSN. This complex coating can act as not only pH-responsive gatekeeper for targeted drug release, but also as an excellent PTT agent for photothermal therapy. Overall, the MSN@MPN nanoplatform shows outstanding drug loading capacity, photothermal property, pH-dependent drug release ability, as well as prominent bio-safety.

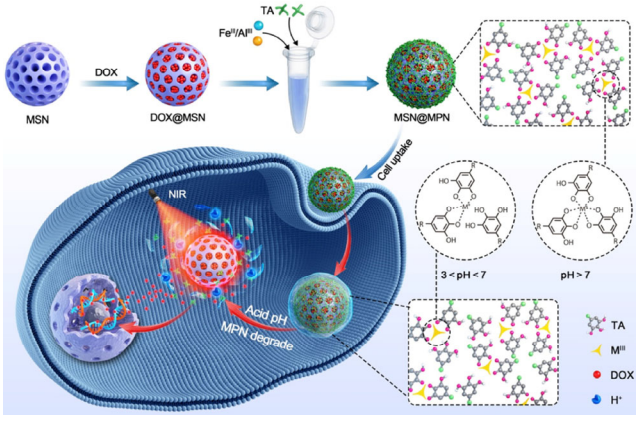

Figure 1 Schematic illustration of the multifunctional MSN@MPN for combinatorial pH-sensitive drug delivery and photothermal therapy.

2 Results and discussion

2.1 Synthesis and characterization of mesoporous silica nanoparticles

Three-dimensional (3D)-MSNs were synthesized by the method of Zhao et al. [37]. Various MSNs with different pore structures were synthesized by using different organic solvents as the upper oil phase, for instance, 1-octadecene, decalin, and cyclohexane. Briefly, the 3D dendritic MSN utilizes cyclohexane as the upper organic phase, while the worm-like MSNs are synthesized using 1-octadecene as the upper organic oil phase.

The morphologies and surface properties of MSNs were investigated by scanning electron microscopy (SEM) and transmission electron microscopy (TEM). The typical low-magnification TEM image in Fig. 2(a) showed the synthesized MSNs were monodisperse nanospheres, which has a dendritic pore structure and highly uniform morphology (Fig. 2(b)). SEM image of 3D dendritic MSNs (Fig. 2(c)) confirmed that the as-prepared nanoparticles are nearly spherical shape, which consisted of closely packed pattern. The diameter of 3D dendritic MSNs shows a narrow size distribution at about 95 nm (Fig. 2(d)), which is in good agreement with the results of the TEM and SEM observation (Figs. 2(a) and 2(c)). On the other hand, MSNs synthesized by 1-octadecene as the upper organic oil phase resulted in monodisperse spheres with a worm-like pore structure (Fig. S1 in the Electronic Supplementary Material (ESM)), which has an average diameter of 110 nm (Fig. S2 in the ESM).

Brunauer–Emmett–Teller (BET) gas sorptometry measurements were used to investigate the surface areas of the MSNs (Fig. S3(a) in the ESM). The adsorption–desorption isotherms were considered to be type IV, which demonstrates that the

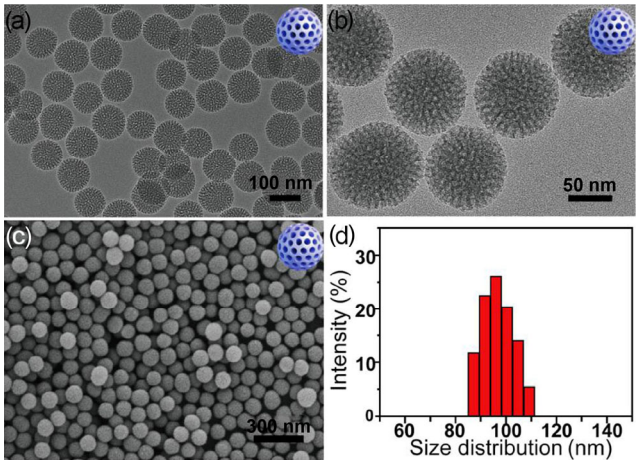

Figure 2 (a) and (b) TEM image of MSNs. (c) SEM image of MSNs. (d) Size distribution of MSNs.

as-prepared MSNs have the typical characteristics of mesoporous materials. BET specific surface area of the sample was determined to be 526.26 m^2/g, and the total pore volume is 0.973 cm^3/g (Fig. S3(b) in the ESM). Large specific surface area and large pore size are conducive to the adsorption and loading of drug molecules [38–40]. These results suggest the 3D dendritic MSN could be used as an excellent drug carrier.

2.2 Characterization of MSN@MPN

MSN@MPN was synthesized via a simple and versatile super-assembly approach. By simply mixing the 3D dendritic MSNs with aqueous solutions containing TA and metal ions, the strong adhesion of TA and complexation between TA and metal ions induced rapid MPN film formation on the surface of MSNs. TEM image of MSN@MPN NPs (Figs. 3(a) and 3(b)) confirmed a thin layer of complex coating was formed on the MSN surface. The size distribution (Fig. 3(c)) indicates that the particle size of MSN@MPN NPs is slightly larger than that of MSN due to the coating of MPN complex.

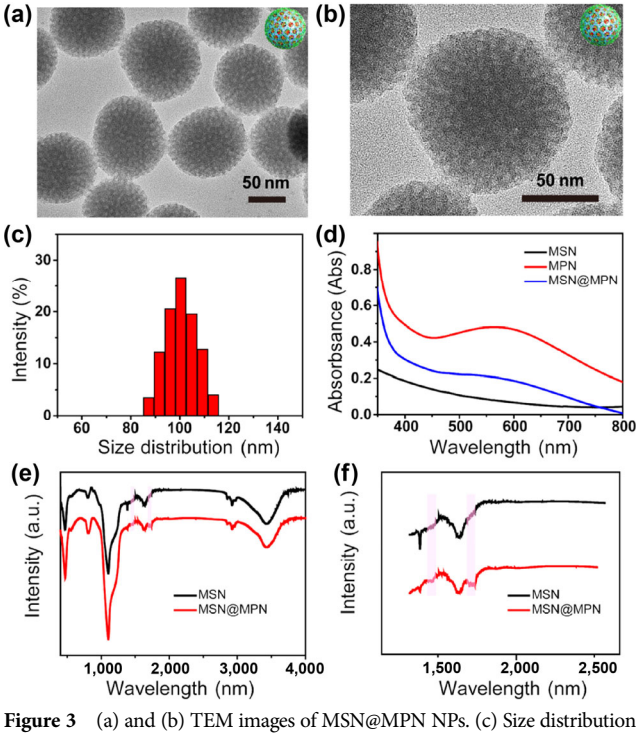

Figure 3 (a) and (b) TEM images of MSN@MPN NPs. (c) Size distribution of MSN@MPN NPs. (d) UV–vis spectra of MSN, MPN and MSN@MPN. ((e) and (f)) FTIR spectra of MSN and MSN@MPN.

The UV–Vis spectra (Fig. 3(d)) showed the MPN coating has a broad absorption peak at about 560 nm, which is due to the formation of FeIII-TA tri-complexes accompanied by the charge transfer from tannic acid to iron ions [41, 42]. MSN@MPN has a similar absorption peak, indicating that MPN coating has been formed in the presence of MSNs. In addition, MSN@MPN exhibits a dark purple color instead of lacte color of pure MSNs (Fig. S3 in the ESM), further confirming the formation of MPN coating on the MSNs. FT-IR analysis provides the evidence of MSNs surface modification (Figs. 3(e) and 3(f)). The peaks from 1,410 to 1,450 cm^{-1} could be designated to the stretching vibration of –C–O– in TA, while the stretching vibration of –C=O– could be confirmed by peaks from 1,630 to 1,740 cm^{-1}. These results reveal that the MPN complex was successfully coated on the surface of MSNs. Further evidence for MSN coating with MPN was confirmed by EDS (Fig. S4 in the ESM). The main elements of silicon (Si), oxygen (O), carbon (C) were observed before coating with MPN film, while the iron (0.38%) and aluminum (0.13%) signals can be detected after the MPN coating procedure.

2.3 Photothermal performance of MSN@MPN

2.3.1 *Photothermal performance of MSN@MPN with different coating layers*

To investigate the effect of MPN coating numbers on photothermal performance of MSN@MPN, aqueous suspensions of MSN@MPN with different coating cycles were prepared and investigated. Figure S6 in the ESM shows the temperature profiles of MSN@MPN aqueous suspension at different coating numbers upon near-infrared laser irradiation, the temperature of MSN@MPN5 (5 MPN coating cycles) aqueous suspension can be gradually raised to 66.3 °C, while MSN@MPN1 (1 MPN coating cycle) aqueous suspension can only be raised to 37.9 °C under the same conditions. This result indicates that the temperature of MSN@MPN aqueous suspension increases rapidly with the coating time. It also reveals that the MPN complex is a vital factor in the photothermal conversion of MSN@MPN.

The thickness of the MPN film increases with the number of coating cycles, which could affect the cumulative release of the drugs. Therefore, it is necessary to control the number of coating cycles to ensure that a good photothermal effect is achieved while the drug can be cumulatively released. MSN@MPN4 can rise up to 60.9 °C (Fig. S6(a) in the ESM), which can effectively kill cancer cells (cancer cells can be killed at 42 to 47 °C). Therefore we further research the drug release performance and photothermal properties of MSN@MPN4.

2.3.2 *Photothermal performance*

In order to evaluate the photothermal performance of MSN@MPN, the temperature elevation profiles for samples at different nanoparticle concentrations were measured by laser irradiation at 808 nm (Fig. 4(a)). At a 2 W/cm^2 laser irradiation for 10 min, the temperatures of MSN@MPN suspensions at a concentration of 0.8, 0.4, 0.2 and 0.1mg/mL can reach up to 61.1, 57.2, 53.1 and 47.1 °C, respectively, while no significant change was observed for pure aqueous solution. Figure 4(b) shows the corresponding infrared (IR) thermographic images acquired for MSN@MPN NPs with different concentrations at 0–10 min. These results indicated that the MSN@MPN possess outstanding photothermal properties.

2.3.3 *Photothermal stability*

To assess the photothermal stability of MSN@MPN, 1 mL of MSN@MPN aqueous suspension (0.4 mg/mL) was irradiated under 808 nm NIR laser for 10 min, then the laser was turned off.

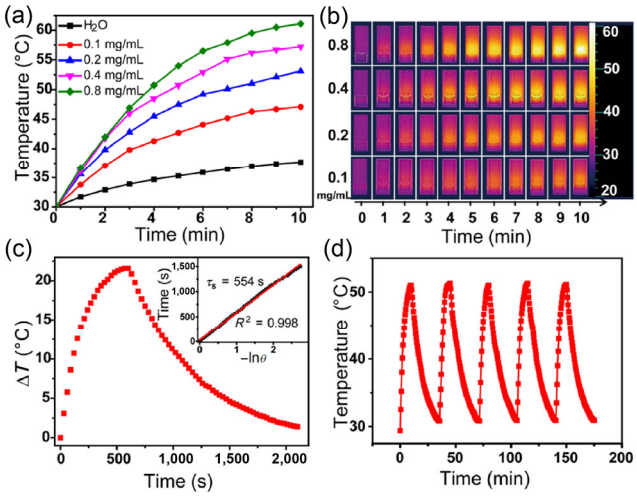

Figure 4 (a) Photothermal curve of MSN@MPN. (b) Corresponding IR thermographic images for MSN@MPN with different concentrations. (c) Irradiation for 600 s followed by the cooling period, the temperature change of MSN@MPN (The inset shows the time constant for heat transfer in this system). (d) Photothermal curve of MSN@MPN with five irradiation on/off cycles.

The time constant (τs) for MSN@MPN system heat transfer was calculated by applying the linear time-dependent data collected during the naturally cooling time. As shown in Fig. 4(c), when irradiated at 808 nm laser for 10 min, the temperature increment of MSN@MPN aqueous solution was 21.6 °C. The time constant for heat transfer from the MSN@MPN system is determined to be 554 s. The photostability of MSN@MPN was researched by using laser irradiation every 25 min over five on/off cycles. As show in Fig. 4(d), the photothermal conversion performance of the MSN@MPN was well maintained after five continuous laser-on/laser-off cycles. In addition, there was no significant change in the temperature increment profiles of MSN@MPN after five cycles. The excellent photothermal conversion performance and prominent photothermal stability indicate MSN@MPN as an effective photothermal agent.

2.4 Loading of doxorubicin (DOX)

DOX is used as a model drug and was loaded into the MSN pores via physical entrapment and electrostatic interaction between the positively charged DOX and negatively charged MSNs. To maximize drug encapsulation, DOX and MSNs were mixed and stirred overnight at 37 °C. Then the drug-loaded particle (MSN-DOX) was collected by centrifugation and washed three times with DI water to remove the redundant DOX on the surface of MSNs. Finally, MSN-DOX was re-dispersed in aqueous solution for MPN coating. In Fig. S8 in the ESM, the zeta potential of different materials shows the change of functional groups on the surface of nanoparticles, which proves the success of the above steps. However, the DOX loading efficiency (LE) was determined to be as low as 10.3% and encapsulation efficiency (EE) was 44.2%. To achieve high loading and encapsulation efficiency, a modified MPN coating method was developed by mixing the MSN-DOX suspension with $FeCl_3$, $AlCl_3$ and TA solution under ultrasonication. The obtained DOX-MSN@Fe/Al-TA was collected by centrifugation and then washed three times with DI water. The loading efficiency and encapsulation efficiency of MSN@MPN for DOX was determined to be 15.7% and 68.2%, respectively.

2.5 pH stimulus-responsive behavior

FeIII-TA complex can degrade at a pH range of 3.0–4.0 [43, 44] while the acidic microenvironment found in most of solid

tumors is at a higher pH (5.0–6.5). Therefore, we introduced AlIII into the FeIII-TA complex to adjust its degradation profile at a pH range of 5.0–6.5 matching the solid tumor microenvironments. The drug release behavior of the mixed ion MSN@MPN was then studied in phosphate buffers at different pH conditions. We first studied the decomposition behavior of MPN films at pH 5.0, 6.0 and 7.4, which simulate the environment of the lysosome, intracellular endosome, and extracellular fluid, respectively [45, 46]. Figure 5(b) shows *in vitro* release profiles at different pH phosphate buffers. The cumulated amount of DOX release from MSN@MPN is less than 25% within 60 h at neutral environment (pH 7.4), while it can reach to 44.2% and 75.6% at pH 6.0 and 5.0, respectively. The pH-dependent drug release of MSN@MPN can be explained by previous reports, while at pH above 7.0, the dominate form of TA-metal ion coordination is tri-coordinated complex, while at pH values less than 7.0 a di-coordinated or mono-coordinated complex was formed [43]. The results demonstrate that MSN@MPN nanoparticles have a pH-triggered targeting drug release behavior. Consequently, MSN@MPN nanoparticles can not only reduce the loss of drugs before reaching the tumor tissue, but also introduces the synergistic effect of chemotherapy and photothermal therapy. The acidic pH environment promotes drug release and significantly improves the efficiency for tumor therapy.

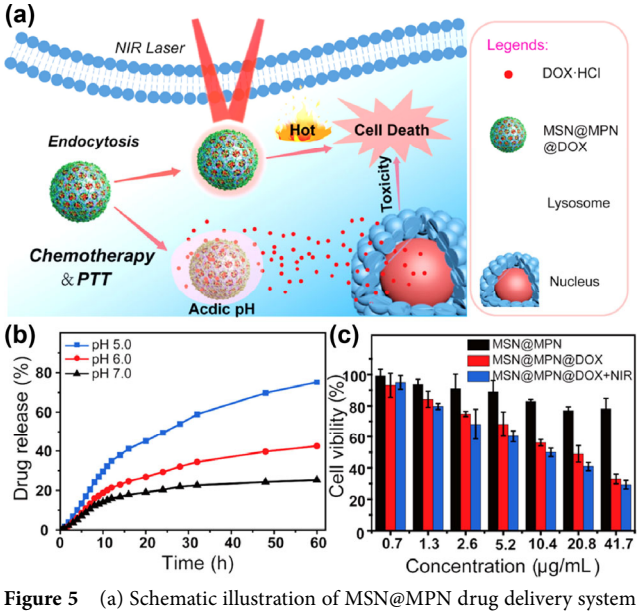

Figure 5 (a) Schematic illustration of MSN@MPN drug delivery system for synergistic photothermal/chemotherapy of cancer. (b) Release profiles of DOX from MSN@MPN at different pH values. (c) Cytotoxicity assay of samples on A549 cells.

2.6 Cell viability studies

To assess the cytotoxicity of the nanoplatform, CCK-8 standard tests were performed on the MSN@MPN system (Fig. 5(c)). At the concentration of 41.7 μg/mL, MSN@MPN NPs did not show significant cytotoxicity to A549 cells, which indicates MSN@MPN nanoplatform has a good biocompatible potential. At the same time, DOX-loaded MSN@MPN and DOX-loaded MSN@MPN with laser irradiation can significantly inhibit the proliferation of A549 cells at the same concentration. The half maximum inhibitory concentration (IC50) of DOX-loaded MSN@MPN and DOX-loaded MSN@MPN with laser irradiation can be calculated as 23.89 and 19.82 μg/mL, respectively. The experimental results showed that DOX-loaded MSN@MPN has a significant inhibitory effect on A549 cells, and the auxiliary laser irradiation can promote the inhibition of A549 cells and enhance the therapeutic effect.

2.7 Cellular uptake studies

Inspired by the superior drug loading capacity and biocompatibility of MSN@MPN NPs, we further researched the cellular uptake and intracellular drug release behaviors using A549 cells.

A549 cells were incubated with DOX-loaded MSN@MPN NPs. As shown in confocal microscopy images of A549 cells in Fig. 6, the red fluorescence signals from DOX can be detected in the cell nuclei, proving that DOX can enter into cells and accumulate in the nucleus. The results revealed that the DOX-loaded MSN@MPN NPs can effectively transport DOX into cells and release the drug under the slight acidic intracellular environments, allowing the drugs to enter the nucleus and leading to programmed apoptosis.

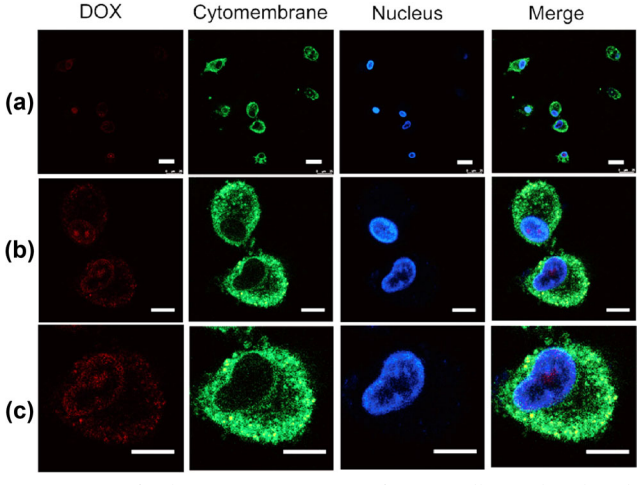

Figure 6 Confocal microscopy images of A549 cells incubated with DOX@MSN@MPN for 6 h at the concentration of 10 μg/mL at pH 7.4 (scale bars: group (a) is 25 μm; group (b) and (c) is 10 μm).

3 Conclusions

In summary, we have developed a new class of pH and photothermal combinatorial therapeutic drug delivery system based on a simple and rapid synthesis strategy of polyphenol-metal ion complex. *In vitro* experiments demonstrated the MSN@MPN system with extremely high drug loading capacity, pH-triggered drug release property and excellent photothermal property. *In vitro* cell studies verified that the MSN@MPN NPs possessed excellent stability and outstanding biocompatibility at physiological environment. This multifunctional nanoplantform can not only be used as photothermal agent for photothermal therapy, but also as an ideal drug carrier for pH-sensitive therapy, allowing further biomedical applications to be explored.

4 Experimental sections

4.1 Synthesis of MSNs

3D-MSNs were synthesized in a biphase stratification method reported by Zhao et al. [37]. In detail, tetraethyl orthosilicate (TEOS) as the silicon source was mixed with hydrophobic organic solvent as the upper oil phase. The lower aqueous phase constitutes triethanolamine and cyltrimethylammonium chloride (CTAC) aqueous solution, wherein CTAC as the template-directing agent, triethanolamine (TEA) as the catalyst. MSNs with different pore structure were prepared by changing the hydrophobic organic reagent in the upper phase. 3D-MSNs with dendritic pore structure were prepared using cyclohexane

as an organic solvent. Briefly, 0.18 g of TEA and 24 mL of CTAC aqueous solution (25 wt.% in H_2O) was added into 36 mL of deionized water, successively. The obtained solution was stirred for 1 h in oil bath at 60 °C. After mixing, 4 mL of TEOS in cyclohexane (20 v/v %) was added to the mixed solution carefully. Then the reaction was kept under magnetic stirring at 60 °C for 12 h. The product was centrifuged at 12,000 rpm for 15 min and then washed with DI water for several times to remove the residual reactants. 3D-MSNs with worm-like pore structure were prepared using 1-octadecene as the hydrophobic organic solvent. The surfactant was removed by extraction three times. Briefly, the as-synthesized MSNs were transferred to 50 mL of ethanol solution containing 0.3 g of NH_4NO_3 and stirred in oil bath at 60 °C for 12 h.

4.2 Synthesis of MSN@MPN nanoparticles

The MSN@MPN nanoparticles were synthesized according to previous reports [13, 43, 47]. Briefly, 10 μL of TA and 10 μL of $AlCl_3$/$FeCl_3$ (24 mM) solution were added to 1 mL (0.5 mg/mL) of MSN aqueous solution under vigorous vortex mixing. Finally, 1 mL of MOPS buffer (20 mM, pH = 8.0) was added to adjust the pH of the solution. Then MSN@MPN were collected by centrifugation and washed with DI water three times.

To research the effect of coating layer on photothermal performance of MSN@MPN, multi-layer coated MSN@MPN were obtained by repeating the coating procedure several times. The MSN coated with MPN complex once was named as MSN@MPN1, MSN coated with MPN complex twice was named MSN@MPN2, and so on. The effect for different coating layer on the photothermal performance of MPN complex was evaluated by recording the temperature change under laser irradiation (808 nm, 2 W/cm^2). The temperature change was monitored every 30 s and the corresponding thermal images at 0 to 8 min were recorded via a thermal FLIR C2 camera.

4.3 Photothermal properties of MSN@MPN

The aqueous solution of MSN@MPN at different concentrations (0, 0.1, 0.2, 0.4 and 0.8 mg/mL) were placed in vials and irradiated with NIR laser (808 nm, 2 W/cm^2) for 10 min. The temperature change and corresponding thermal images were monitored via an infrared thermal camera (Thermal FLIR C2). The photothermal stability of MSN@MPN was evaluated according to previous reports [48, 49]. Briefly, 1 mL of MSN@MPN aqueous solution was irradiated under NIR laser (808 nm, 2 W/cm^2) for 600 s, then the laser was turned off for 25 min. The temperature change of the solution was monitored by thermal FLIR C2 camera. The time constant (τs) for heat transfer was calculated by applying the linear time-dependent data collected during the cooling period. The operation for laser "turn-on" and "turn-off" cycles was repeated for five times to evaluate the photothermal stability of MSN@MPN.

4.4 Loading of DOX

Briefly, 5 mg of DOX and 10 mg of 3D MSNs were soaked in 2 mL DI water. Then the mixture was stirred at 37 °C for 12 h in dark. Then the DOX-loaded MSN@MPN nanoparticles were synthesized by the method reported in Refs. [13, 43, 47]. 10 μL of TA (24 mM) solution and 10 μL of $AlCl_3$/$FeCl_3$ (24 mM)) solution was added to 1 mL (0.5 mg/mL) of DOX-MSN aqueous suspension under vigorous mixing. Then 1 mL of MOPS buffer (20 mM, pH 8.0) was added to adjust the pH of the solution. Then DOX-MSN@MPN were collected by centrifugation and washed with DI water 3 times. The final product was separated by centrifugation, washed with DI water and dried. The DOX loading capacity was determined by UV–vis spectrophotometer. The DOX loading efficiency and encapsulation efficiency were calculated by Eqs. (1) and (2) as follows

$$\text{Drug loading efficiency (\%)} = (\text{quality of drug loaded})/(\text{quality of drug loaded nanoparticles}) \times 100\% \quad (1)$$

$$\text{Drug encapsulation efficiency (\%)} = (\text{quality of drug loaded})/(\text{total quality of feeding drug}) \times 100\% \quad (2)$$

4.5 *In vitro* drug release of MSN@MPN

In vitro drug release of MSN@MPN was studied by dispersing DOX-loaded MSN@MPN nanoparticles in PBS buffer at different pH (PBS, 0.01 M, pH= 7.4, 6.0 and 5.0). In brief, 5 mL of DOX·HCl-loaded MSN@MPN nanoparticles (2 mg/mL) were added into dialysis bags (MWCO 13,000) which were soaked separately in 45 mL of PBS solution stirred at 140 rpm, 37 °C. Then, 5 mL of external buffer solution was drawn out at appropriate intervals for test and supplemented with the same volume of fresh buffer solution. The concentration of DOX was measured by fluorescence spectrophotometer.

4.6 *In vitro* cell viability assay of MSN@MPN NPs

In vitro cytoviability of MSN@MPN and DOX-loaded MSN@MPN was evaluated by standard CCK-8 method using A549 cells. Briefly, A549 cells were seeded in 96-well plates with an initial density of 5,400 cells/well and incubated in 100 μL of DMEM at 37 °C for 24 h. Subsequently, 10 μL of MSN@MPN, DOX-loaded MSN@MPN solution at various nanoparticles concentrations were added into each well, respectively. Cells incubated with free of nanoparticles and blank DMEM were used as controls. After 24 h incubation, 10 μL of CCK-8 solution was added to the cells followed by incubation at 37 °C for additional 4 h. The optical density (OD) value of CCK-8 assay was determined with a spectrophotometric microplate reader at 450 nm. The relative cells viability was calculated with the equation:

$$\text{Cell viability (\%)} = (A(\text{DOX-loaded MSN@MPN}) - A(\text{blank1}))/(A(\text{blank2}) - A(\text{blank3})) \times 100\%$$

Whereas A(DOX-loaded MSN@MPN) is the absorbance values of medium that containing DOX-loaded MSN@MPN nanoparticles and cells. A(blank1) is the control group the medium containing DOX-loaded MSN@MPN nanoparticles without cells. A(blank3) is the absorbance values of blank medium. Experimental group (A(DOX-loaded MSN@MPN) and A(MSN@MPN) were presented as average ± SD (n = 3)).

4.7 Cellular uptake of DOX-loaded MSN@MPN NPs

To investigate the cellular uptake efficiency of MSN@MPN NPs, A549 (human lung cancer cell line) cells were seeded in DMEM medium (1.5 mL) containing 10% fetal bovine serum (FBS) and inoculated into confocal dish and cultured in an incubator for 24 h. Subsequently, removed medium and equivoluminal medium containing DOX-loaded NPs was added. After 6 hours of incubation, the cells were imaged under a confocal laser scanning microscope (CLSM).

Acknowledgements

This work was supported by the National Key Research and Development Program of China (Nos. 2019YFC1604600, 2017YFA0206901, 2017YFA0206900), the National Natural Science Foundation of China (Nos. 21705027, 21974029, and 81830052), the Construction project of Shanghai Key Laboratory of Molecular Imaging (No. 18DZ2260400), the Shanghai Municipal Education Commission (Class II Plateau Disciplinary Construction Program of Medical Technology of SUMHS,

2018-2020), the Australia National Health and Medical Research Council (NHMRC) (No. APP1163786), the Scientia Fellowship program at UNSW, the MCTL Visiting Fellowship Program, Shanghai Key Laboratory of Molecular Imaging (No. 18DZ2260400), the Natural Science Foundation of Shanghai, and the Recruitment Program of Global Experts of China and Shanghai.

Electronic Supplementary Material: Supplementary material (TEM measurements, particle distribution, N_2 adsorption–desorption isotherm, photographs images, SEM-EDS elemental analysis, photothermal conversion curve and TGA curves) is available in the online version of this article at https://doi.org/10.1007/s12274-020-2736-6.

References

[1] Liu, Y. L.; Ai, K. L.; Liu, J. H.; Deng, M.; He, Y. Y.; Lu, L. H. Dopamine-melanin colloidal nanospheres: An efficient near-infrared photothermal therapeutic agent for *in vivo* cancer therapy. *Adv. Mater.* **2013**, *25*, 1353–1359.

[2] Fan, J. X.; Zheng, D. W.; Mei, W. W.; Chen, S.; Chen, S. Y.; Cheng, S. X.; Zhang, X. Z. A metal-polyphenol network coated nano-theranostic system for metastatic tumor treatments. *Small* **2017**, *13*, 1702714.

[3] Jiang, Y. J.; Liu, S. J.; Zhang, Y.; Li, H. C.; He, H.; Dai, J. T.; Jiang, T.; Ji, W. H.; Geng, D. Y.; Elzatahry, A. A. et al. Magnetic mesoporous nanospheres anchored with LyP-1 as an efficient pancreatic cancer probe. *Biomaterials* **2017**, *115*, 9–18.

[4] Yang, J. P.; Shen, D. K.; Zhou, L.; Li, W.; Li, X. M.; Yao, C.; Wang, R.; El-Toni, A. M.; Zhang, F.; Zhao, D. Y. Spatially confined fabrication of core–shell gold nanocages@mesoporous silica for near-infrared controlled photothermal drug release. *Chem. Mater.* **2013**, *25*, 3030–3037.

[5] Chen, W. S.; Ouyang, J.; Liu, H.; Chen, M.; Zeng, K.; Sheng, J. P.; Liu, Z. J.; Han, Y. J.; Wang, L. Q.; Li, J. et al. Black phosphorus nanosheet-based drug delivery system for synergistic photodynamic/photothermal/chemotherapy of cancer. *Adv. Mater.* **2017**, *29*, 1603864.

[6] Liu, Y.; Yin, J. J.; Nie, Z. H. Harnessing the collective properties of nanoparticle ensembles for cancer theranostics. *Nano Res.* **2014**, *7*, 1719–1730.

[7] Chen, G. J.; Jaskula-Sztul, R.; Esquibel, C. R.; Lou, I.; Zheng, Q. F.; Dammalapati, A.; Harrison, A.; Eliceiri, K. W.; Tang, W. P.; Chen, H. et al. Neuroendocrine tumor-targeted upconversion nanoparticle-based micelles for simultaneous NIR-controlled combination chemotherapy and photodynamic therapy, and fluorescence imaging. *Adv. Funct. Mater.* **2017**, *27*, 1604671.

[8] Lin, L. S.; Song, J. B.; Yang, H. H.; Chen, X. Y. Yolk-shell nanostructures: Design, synthesis, and biomedical applications. *Adv. Mater*. **2018**, *30*, 1704639.

[9] Zeng, J. Y.; Zhang, M. K.; Peng, M. Y.; Gong, D.; Zhang, X. Z. Porphyrinic metal-organic frameworks coated gold nanorods as a versatile nanoplatform for combined photodynamic/photothermal/chemotherapy of tumor. *Adv. Funct. Mater.* **2018**, *28*, 1705451.

[10] Poulose, A. C.; Veeranarayanan, S.; Mohamed, M. S.; Nagaoka, Y.; Aburto, R. R.; Mitcham, T.; Ajayan, P. M.; Bouchard, R. R.; Sakamoto, Y.; Yoshida, Y. et al. Multi-stimuli responsive Cu_2S nanocrystals as trimodal imaging and synergistic chemo-photothermal therapy agents. *Nanoscale* **2015**, *7*, 8378–8388.

[11] Fang, S.; Lin, J.; Li, C. X.; Huang, P.; Hou, W. X.; Zhang, C. L.; Liu, J. J.; Huang, S. S.; Luo, Y. X.; Fan, W. P. et al. Dual-stimuli responsive nanotheranostics for multimodal imaging guided trimodal synergistic therapy. *Small* **2017**, *13*, 1602580.

[12] Gulzar, A.; Xu, J. T.; Xu, L. G.; Yang, P. P.; He, F.; Yang, D.; An, G. H.; Ansari, M. B. Redox-responsive UCNPs-DPA conjugated NGO-PEG-BPEI-DOX for imaging-guided PTT and chemotherapy for cancer treatment. *Dalton Trans.* **2018**, *47*, 3921–3930.

[13] Ping, Y.; Guo, J. L.; Ejima, H.; Chen, X.; Richardson, J. J.; Sun, H. L.; Caruso, F. pH-responsive capsules engineered from metal-phenolic networks for anticancer drug delivery. *Small* **2015**, *11*, 2032–2036.

[14] Hu, C. L.; Huang, P.; Zheng, Z.; Yang, Z. B.; Wang, X. L. A facile strategy to prepare an enzyme-responsive mussel mimetic coating for drug delivery based on mesoporous silica nanoparticles. *Langmuir* **2017**, *33*, 5511–5518.

[15] Zhu, X. L.; Huang, H. Q.; Zhang, Y. J.; Zhang, H. J.; Hou, L.; Zhang, Z. Z. Cit/CuS@Fe_3O_4-based and enzyme-responsive magnetic nanoparticles for tumor chemotherapy, photothermal, and photodynamic therapy. *J. Biomater. Appl.* **2017**, *31*, 1010–1025.

[16] Su, Y.; Ojo, O. F.; Tsengam, I. K. M.; He, J. B.; McPherson, G. L.; John, V. T.; Valla, J. A. Thermoresponsive coatings on hollow particles with mesoporous shells serve as stimuli-responsive gates to species encapsulation and release. *Langmuir* **2018**, *34*, 14608–14616.

[17] Bathfield, M.; Reboul, J.; Cacciaguerra, T.; Lacroix-Desmazes, P.; Gérardin, C. Thermosensitive and drug-loaded ordered mesoporous silica: A direct and effective synthesis using PEO-b-PNIPAM block copolymers. *Chem. Mater.* **2016**, *28*, 3374–3384.

[18] Park, K.; Park, S. S.; Yun, Y. H.; Ha, C. S. Mesoporous silica nanoparticles functionalized with a redox-responsive biopolymer. *J. Porous Mater.* **2017**, *24*, 1215–1225.

[19] Li, C. X.; Zhang, Y. F.; Li, Z. M.; Mei, E. C.; Lin, J.; Li, F.; Chen, C. G.; Qing, X. L.; Hou, L. Y.; Xiong, L. L. et al. Light-responsive biodegradable nanorattles for cancer theranostics. *Adv. Mater.* **2018**, *30*, 1706150.

[20] Giri, S.; Trewyn, B. G.; Stellmaker, M. P.; Lin, V. S. Y. Stimuli-responsive controlled-release delivery system based on mesoporous silica nanorods capped with magnetic nanoparticles. *Angew. Chem., Int. Ed.* **2005**, *44*, 5038–5044.

[21] Li, S.; Wu, W.; Xiu, K. M.; Xu, F. J.; Li, Z. M.; Li, J. S. Doxorubicin loaded pH-responsive micelles capable of rapid intracellular drug release for potential tumor therapy. *J. Biomed. Nanotechnol.* **2014**, *10*, 1480–1489.

[22] Chen, T. C.; Wu, W.; Xiao, H.; Chen, Y. X.; Chen, M.; Li, J. S. Intelligent drug delivery system based on mesoporous silica nanoparticles coated with an ultra-pH-sensitive gatekeeper and poly(ethylene glycol). *ACS Macro Lett.* **2016**, *5*, 55–58.

[23] Wang, Z. T.; Huang, P.; Jacobson, O.; Wang, Z.; Liu, Y. J.; Lin, L. S.; Lin, J.; Lu, N.; Zhang, H. M.; Tian, R. et al. Biomineralization-inspired synthesis of copper sulfide-ferritin nanocages as cancer theranostics. *ACS Nano* **2016**, *10*, 3453–3460.

[24] Lin, J.; Wang, M.; Hu, H.; Yang, X. Y.; Wen, B.; Wang, Z. T.; Jacobson, O.; Song, J. B.; Zhang, G. F.; Niu, G. et al. Multimodal-imaging-guided cancer phototherapy by versatile biomimetic theranostics with UV and γ-irradiation protection. *Adv. Mater.* **2016**, *28*, 3273–3279.

[25] Wang, D. D.; Dong, H. F.; Li, M.; Cao, Y.; Yang, F.; Zhang, K.; Dai, W. H.; Wang, C. T.; Zhang, X. J. Erythrocyte-cancer hybrid membrane camouflaged hollow copper sulfide nanoparticles for prolonged circulation life and homotypic-targeting photothermal/chemotherapy of melanoma. *ACS Nano* **2018**, *12*, 5241–5252.

[26] Liu, Y.; Zhen, W. Y.; Jin, L. H.; Zhang, S. T.; Sun, G. Y.; Zhang, T. Q.; Xu, X.; Song, S. Y.; Wang, Y. H.; Liu, J. H. et al. All-in-one theranostic nanoagent with enhanced reactive oxygen species generation and modulating tumor microenvironment ability for effective tumor eradication. *ACS Nano* **2018**, *12*, 4886–4893.

[27] Meng, Z. Q.; Chao, Y.; Zhou, X. F.; Liang, C.; Liu, J. J.; Zhang, R.; Cheng, L.; Yang, K.; Pan, W.; Zhu, M. F. et al. Near-infrared-triggered *in situ* gelation system for repeatedly enhanced photothermal brachytherapy with a single dose. *ACS Nano* **2018**, *12*, 9412–9422.

[28] Shi, D. L.; Cho, H. S.; Chen, Y.; Xu, H.; Gu, H. C.; Lian, J.; Wang, W.; Liu, G. K.; Huth, C.; Wang, L. M. et al. Fluorescent polystyrene-Fe_3O_4 composite nanospheres for *in vivo* imaging and hyperthermia. *Adv. Mater.* **2009**, *21*, 2170–2173.

[29] Yoo, D.; Jeong, H.; Noh, S. H.; Lee, J. H.; Cheon, J. Magnetically triggered dual functional nanoparticles for resistance-free apoptotic hyperthermia. *Angew. Chem., Int. Ed.* **2013**, *52*, 13047–13051.

[30] Ding, Q.; Liu, D. F.; Guo, D. W.; Yang, F.; Pang, X. Y.; Che, R C.; Zhou, N. Z.; Xie, J.; Sun, J. F.; Huang, Z. H. et al. Shape-controlled fabrication of magnetite silver hybrid nanoparticles with high performance magnetic hyperthermia. *Biomaterials* **2017**, *124*, 35–46.

[31] Wang, C.; Sun, W. J.; Wright, G.; Wang, A. Z.; Gu, Z. Inflammation-triggered cancer immunotherapy by programmed delivery of CpG and anti-PD1 antibody. *Adv. Mater.* **2016**, *28*, 8912–8920.

[32] Oberli, M. A.; Reichmuth, A. M.; Dorkin, J. R.; Mitchell, M. J.; Fenton,

O. S.; Jaklenec, A.; Anderson, D. G.; Langer, R.; Blankschtein, D. Lipid nanoparticle assisted mRNA delivery for potent cancer immunotherapy. *Nano Lett.* **2017**, *17*, 1326–1335.

[33] Yu, G. T.; Rao, L.; Wu, H.; Yang, L. L.; Bu, L. L.; Deng, W. W.; Wu, L.; Nan, X. L.; Zhang, W. F.; Zhao, X. Z. et al. Myeloid-derived suppressor cell membrane-coated magnetic nanoparticles for cancer theranostics by inducing macrophage polarization and synergizing immunogenic cell death. *Adv. Funct. Mater.* **2018**, *28*, 1801389.

[34] Phuengkham, H.; Song, C.; Um, S. H.; Lim, Y. T. Implantable synthetic immune niche for spatiotemporal modulation of tumor-derived immunosuppression and systemic antitumor immunity: Postoperative immunotherapy. *Adv. Mater.* **2018**, *30*, 1706719.

[35] Dong, Q.; Wang, X. W.; Hu, X. X.; Xiao, L. Q.; Zhang, L.; Song, L. J.; Xu, M. L.; Zou, Y. X.; Chen, L.; Chen, Z. et al. Simultaneous application of photothermal therapy and an anti-inflammatory prodrug using pyrene-aspirin-loaded gold nanorod graphitic nanocapsules. *Angew. Chem., Int. Ed.* **2018**, *57*, 177–181.

[36] Chen, S.; Lei, Q.; Qiu, W. X.; Liu, L. H.; Zheng, D. W.; Fan, J. X.; Rong, L.; Sun, Y. X.; Zhang, X. Z. Mitochondria-targeting "Nanoheater" for enhanced photothermal/chemo-therapy. *Biomaterials* **2017**, *117*, 92–104.

[37] Shen, D. K.; Yang, J. P.; Li, X. M.; Zhou, L.; Zhang, R. Y.; Li, W.; Chen, L.; Wang, R.; Zhang, F.; Zhao, D. Y. Biphase stratification approach to three-dimensional dendritic biodegradable mesoporous silica nanospheres. *Nano Lett.* **2014**, *14*, 923–932.

[38] Chen, Y.; Chen, H. R.; Shi, J. L. *In vivo* bio-safety evaluations and diagnostic/therapeutic applications of chemically designed mesoporous silica nanoparticles. *Adv. Mater.* **2013**, *25*, 3144–3176.

[39] Luo, Z.; Hu, Y.; Cai, K. Y.; Ding, X. W.; Zhang, Q.; Li, M. H.; Ma, X.; Zhang, B. L.; Zeng, Y. F.; Li, P. Z. et al Intracellular redox-activated anticancer drug delivery by functionalized hollow mesoporous silica nanoreservoirs with tumor specificity. *Biomaterials* **2014**, *35*, 7951–7962.

[40] Schrand, A. M.; Schlager, J. J.; Dai, L. M.; Hussain, S. M. Preparation of cells for assessing ultrastructural localization of nanoparticles with transmission electron microscopy. *Nat. Protoc.* **2010**, *5*, 744–757.

[41] Rahim, M. A.; Ejima, H.; Cho, K. L.; Kempe, K.; Müllner, M.; Best, J. P.; Caruso, F. Coordination-driven multistep assembly of metal–polyphenol films and capsules. *Chem. Mater.* **2014**, *26*, 1645–1653.

[42] Ozawa, H.; Haga, M. A. Soft nano-wrapping on graphene oxide by using metal-organic network films composed of tannic acid and Fe ions. *Phys. Chem. Chem. Phys.* **2015**, *17*, 8609–8613.

[43] Ejima, H.; Richardson, J. J.; Liang, K.; Best, J. P.; van Koeverden, M. P.; Such, G. K.; Cui, J. W.; Caruso, F. One-step assembly of coordination complexes for versatile film and particle engineering. *Science* **2013**, *341*, 154–157.

[44] Guo, J. L.; Ping, Y.; Ejima, H.; Alt, K.; Meissner, M.; Richardson, J. J.; Yan, Y.; Peter, K.; von Elverfeldt, D.; Hagemeyer, C. E. et al. Engineering multifunctional capsules through the assembly of metal-phenolic networks. *Angew. Chem., Int. Ed.* **2014**, *53*, 5546–5551.

[45] Chen, W.; Zhong, P.; Meng, F. H.; Cheng, R.; Deng, C.; Feijen, J.; Zhong, Z. Y. Redox and pH-responsive degradable micelles for dually activated intracellular anticancer drug release. *J. Control. Release* **2013**, *169*, 171–179.

[46] Gerweck, L. E.; Seetharaman, K. Cellular pH gradient in tumor versus normal tissue: Potential exploitation for the treatment of cancer. *Cancer Res.* **1996**, *56*, 1194–1198.

[47] Fan, J. X.; Zheng, D. W.; Rong, L.; Zhu, J. Y.; Hong, S.; Li, C.; Xu, Z. S.; Cheng, S. X.; Zhang, X. Z. Targeting epithelial-mesenchymal transition: Metal organic network nano-complexes for preventing tumor metastasis. *Biomaterials* **2017**, *139*, 116–126.

[48] Roper, D. K.; Ahn, W.; Hoepfner, M. Microscale heat transfer transduced by surface plasmon resonant gold nanoparticles. *J. Chem. Phys. C* **2007**, *111*, 3636–3641.

[49] Li, B.; Wang, Q.; Zou, R. J.; Liu, X. J.; Xu, K. B.; Li, W. Y.; Hu, J. Q. $Cu_{7.2}S_4$ nanocrystals: A novel photothermal agent with a 56.7% photothermal conversion efficiency for photothermal therapy of cancer cells. *Nanoscale* **2014**, *6*, 3274–3282.